Available online at www.eccomasproceedia.org
Eccomas Proceedia COMPDYN (2023) 2587-2596

ECCOMAS
Proceedia

COMPDYN 2023
9th ECCOMAS Thematic Conference on
Computational Methods in Structural Dynamics and Earthquake Engineering
M. Papadrakakis, M. Fragiadakis (eds.)
Athens, Greece, 12-14 June 2023

3D NUMERICAL SIMULATIONS OF MULTI-LAYERED ELASTOMERIC BEARINGS (EB) SUBJECTED TO COMBINED VERTICAL AND HORIZONTAL LOADS.

Davide Forcellini[1] **and Konstantinos N. Kalfas**[2]

[1] University of San Marino, Via Salita La Rocca, 44 San Marino, San Marino
e-mail: davide.forcellini@unirsm.sm

[2] Southern Methodist University 3101 Dyer St, Dallas, TX 75205, United States
e-mail: kkalfas@smu.edu

Abstract

Multi-layered elastomeric bearings (EB) have been applied in structural engineering as a mitigation solution for improving the seismic resilience of structural configurations. Such devices have been extensively verified for different loading conditions with laboratory tests and numerical simulations during the last decades. However, their behavior under the mutual effect of axial and shear load is still under assessment. This paper presents the results of 3D numerical simulations of EBs when subjected to large horizontal movements by considering the role of the shear modulus. The paper considers several numerical models of EBs. The main goal is to implement the proposed analytical formulation to numerical platforms that can describe the combined axial – shear macroscopic behavior of the EBs.

Keywords: 3D Numerical Simulations, Multi-Layered Elastomeric Bearings, Interaction, Vertical Loads, Longitudinal Load.

ISSN:2623-3347
Peer-review under responsibility of the organizing committee of COMPDYN 2023.
doi: 10.7712/120123.10585.21044

1 INTRODUCTION

In the last 60 years, base isolation has become a well-known method with many applications to enhance the seismic resilience of many structures all over the world. In particular, elastomeric bearings (EB) have been widely applied to support structures under the mutual effects of axial and horizontal loads. In this regard, analytical formulations have been proposed, such as Haringx [1] who studied the buckling by considering the shear deformation and the buckling theory of beam elements. In Kelly [2] an analytical formulation was developed to study the critical loading and the stability of EBs under axial and horizontal loads. In addition, Kelly and Konstantinidis [3,4] considered the application of pure compression or pure bending to EBs, by considering linear elastic rubbers and infinitesimal strain theory. Experimental studies have been also proposed [5-10] in order to develop formulations that represent the interaction between the axial and the horizontal stiffness under shear deformations. Experimental studies on EBs were conducted by Cardone and Gesualdi [11] with the aim to investigate the role of the air temperature demonstrating that it alters considerably the stress levels and the shear stiffness of the elastomer. In Rastgoo Moghadam and Konstantinidis [12] the behavior of EBs under combined cyclic displacement, axial load, and rotation was investigated. Nagarajaiah and Ferrell, and Kumar *et al.* [13, 14] performed numerical simulations to assess the role of non-linearity in affecting critical and post-critical mechanisms. Numerical studies were performed by Rastgoo Moghadam and Konstantinidis, Kalfas *et al.*, and Kalfas and Mitoulis [15-19] in order to assess the effects of the support rotation on the damage capacity under combined axial and shear loads.

Applications of the seismic isolation technique was investigated by Forcellini *et al.* [20-22]. Applications to bridges were proposed by Gauron *et al.* [23] and Forcellini [24]. Moreover, Forcellini, and Kalfas and Forcellini [25, 26] considered the role of non-linearity for bridges. Rahnavard *et al.*, and Altalabani *et al.* [27, 28] proposed numerical simulations of EBs that apply the rubber cores to increase the lateral stability. In Sheikhi et al. [29, 30] rubber bearings were coupled with dampers and Radkia et al. [31] considered the role of EBs in steel asymmetric structures considering soil-structure interaction. The role of support rotation was object of many contributions [15, 32-35] and some surveys of the major earthquakes in South America and Asia [36, 37] were also proposed. Regarding the support rotation, the European and American design guidelines [38, 39] consider a finite support rotation, i.e., small rotation of the anchor plates, or relative rotation. Forcellini and Kelly [40], Forcellini *et al.*, and Kalfas and Forcellini [24, 25] extensively investigated the role of the rotation on the EBs under the effects of the combined axial and lateral loads. In particular, Forcellini *et al.*, and Kalfas and Forcellini [25, 33] considered the mechanisms induced by the large deformations and the post-buckling behavior of EBs by developing the original model by Koh and Kelly, Kelly, and Kelly and Takhirov [2, 41].

This study proposes 3D numerical simulations and presents the results developed by Kalfas *et al.* [42, 43], where the microscopic model of EBs to assess the role of the shear modulus, G_b, is reproduced. In section 2 the 3D numerical models are described, while the role of the shear modulus, G_b, the relative rotation, θ, and the applied axial compressive load, P, is investigated in section 3, buy comparing with the analytical model proposed by Forcellini and Kelly [40].

2 3D NUMERICAL MODELS

In this paper, the finite element analysis (FEA) software Abaqus [44] was performed on four different case studies of EBs. These models were validated against experimental studies [44] and previous numerical simulations [27]. In Figure 1, the validation with the experimental studies (left) and the numerical ones (right) is displayed. The comparisons are made against the experimental work by [44] and by Rahnavard and Thomas [26] who considered thirty rubber layers (4 mm thickness each), alternating with twenty-nine steel shims (3.1 mm thickness each). At the top and bottom, two anchor plates (28 mm thickness each) were placed. Both the rubber layers and the steel shims had 700 mm diameter when the comparison was against the experiments [44]; while the corresponding diameter was 400 mm when the comparison was against the work of Rahnavard and Thomas [27]. The anchor plates had a diameter of 1000 mm and 500 mm, when the comparison was against the experiments [44] and

against the work of Rahnavard and Thomas [27], respectively. A hole with a diameter of 15 mm designed at the center of the reference EBs.

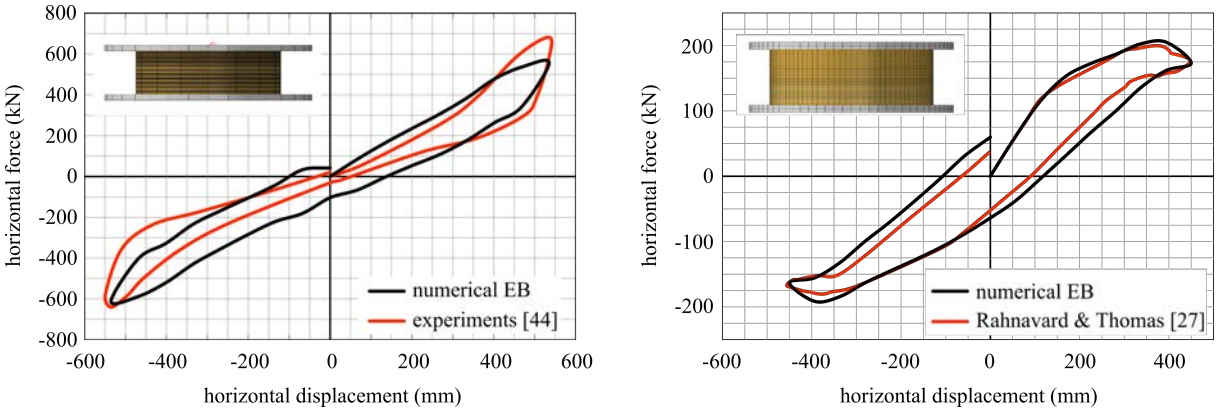

Figure 1. Comparison between the reference EBs numerical models and the experimental results [44] (left); and the work of Rahnavard and Thomas [27] (right).

The hyperelastic material was used for the rubber (in terms of stresses, strains and energy dissipation), by considering three possible models: the Ogden [45], the Neo-Hookean [46] and the Rivlin [47]. It is worth noting that [48] demonstrated that the Rivlin model cannot represent materials that develop strains larger than 200% and that the Ogden hyperelastic material can accurately represent rubber-like materials that reach strains up to 700%. In addition, several numerical studies have considered the Ogden hyperelastic material for EBs [16-18, 26, 33]. Therefore, in this paper this latter material model was considered (more details in [42]) and the properties of the rubber layer (represented as an isotropic material) were a combination of the Ogden hyperelastic material and a hysteretic material model [44, 45, 49].

The validation consisted in comparing the model with the experimental contribution by [44] (Figure 1, left) for a vertical load of 14 MPa, followed by a full cycle of loading-unloading of 535 mm that corresponds to 445% of the total height of rubber (Tr = 120 mm). EB model was validated against Rahnavard and Thomas [26] (Figure 1, right), subjected to a vertical load of 2 MPa, followed by a full cycle of loading-unloading of 455 mm that corresponds to 375% shear strain. It can be seen in Figure 1 the accuracy of the numerical model (solid line) with those representing the experimental one (dashed line) [44]. The mechanical properties of the rubber layers, the steel shims and the anchor plates, are shown in Table 1. The same hysteretic properties, the elastic and plastic properties and the anchor plates were also considered for the other three numerical models of EBs. It is worth noting that the cyclic loop was considered by following those described in [16-18, 26, 33]. In addition, the hysteretic parameters (S_{SF}: stress scaling factor, C: creep strain exponent, m: effective stress exponent, and A: creep parameter) were selected by considering Bergström and Boyce [49]. The same value was applied in the numerical models by [16-19, 25, 33]. The applied initial stiffness parameters (α_1 and μ_1) and the post-elastic stiffness parameters (α_2 and μ_2) and the multiple values of the shear modulus, G_b are shown in Table 2. These values were applied to the reference EB (the $EB_{1,a}$ model). Notice that these models are herein referred as $EB_{1,a}$, $EB_{1,b}$, $EB_{1,c}$ and $EB_{1,d}$, (Table 2). The EB models were built up with C3D8H elements for the rubber layers; while C3D8R brick elements were applied for the steel shims and the anchor plates [44].

Figure 2 shows the geometry of the models ($EB_{1,a}$, $EB_{1,b}$, $EB_{1,c}$, and $EB_{1,d}$) that consist of thirty rubber layers, twenty-nine steel shims and two anchor plates. At the middle of each model there was a hole of 15 mm diameter. The rubber layers had a thickness of 4 mm, the steel shims had a thickness of 3.1 mm, and the anchor plates had a thickness of 28 mm (the total thickness of EBs 56 mm). The diameter of the rubber layers and the steel shims was chosen to be 700 mm; while that of the anchor plates was 1000 mm. The geometric properties are described in Table 3, more details in [42].

rubber layers					
hyperelastic coefficients					
initial stiffness parameters		post-elastic stiffness parameters			
μ1 (MPa)	α1	μ2 (MPa)	α2		
0.41	1.6	0.0012	6.2		
hysteretic parameters					
stress scaling factor	creep strain exponent	effective stress exponent	creep parameter		
SSF	C	m	A		
1.6	-1	4	0.56		
mechanical properties					
shear modulus	Poisson's ratio	bulk modulus			
Gb (MPa)	νr	B (MPa)			
0.66	0.4998	1,000			
steel shims & anchor plates					
Young's modulus	Poisson's ratio	yielding strength	yielding strain	ultimate strength	ultimate strain
E (MPa)	νs	Fy (MPa)	εy	Fu (MPa)	εu
205,000	0.3	235	0.115	350	0.15

Table 1: Material and mechanical properties of rubber and steel layers of EB.

models	initial stiffness parameters		post-elastic stiffness parameters		shear modulus
	μ_1 (MPa)	α_1	μ_2 (MPa)	α_2	G_b (MPa)
$EB_{1,a}$	0.41	1.6	0.0012	6.2	0.66
$EB_{1,b}$	0.389	1.52	0.0011	5.89	0.60
$EB_{1,c}$	0.37	1.456	0.00109	5.64	0.55
$EB_{1,d}$	0.355	1.389	0.00104	5.382	0.50

Table 2: Initial (α1 and μ1) and post-elastic (α2 and μ2) stiffness parameters and shear modulus, Gb, values.

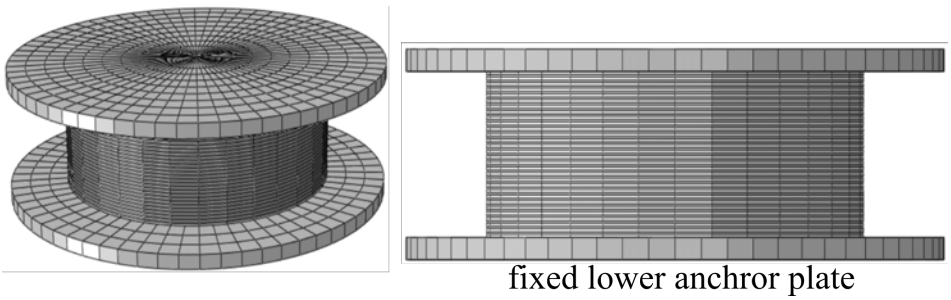

Figure 2. Three-dimensional numerical model (left), and side view (right) of the reference EB1.

models		EB1, a - EB1, d
steel shims	number of layers – ns, i	29
	diameter (mm) – Ds, i	700
	thickness (mm) – ts, i	3.1
	total thickness (mm) – Ts, i	89.9
rubber layer	number of layers – nr, i	30
	diameter (mm) – Dr, i	700
	thickness (mm) – tr, i	4
	total thickness (mm) – Tr, i	120
anchor plate	number of layers – nap, i	2
	diameter (mm) – Dap, i	1000
	thickness (mm) – tap, i	28
	total thickness (mm) – Tap, i	56
shape factor – Si		44
total height – Ti		265.9
diameter of center hole – Dh, i		15

* where i is equal to 1, a; 1, b; 1, c; and 1, d, depending on the model of the EB

Table 3: Mesh sizes of the different components of the EBs and sensitivity analysis results compared to the experimental effective stiffness.

3 THE ROLE OF THE SHEAR MODULUS

The role of the shear modulus, G_b was investigated herein. In particular, the load-displacement curves (hysteretic loops) of the different EB numerical models ($EB_{1,a}$, $EB_{1,b}$, $EB_{1,c}$, and $EB_{1,d}$) at various values of G_b (0.66, 0.60, 0.55 and 0.50 MPa, respectively) and subjected to different applied axial compressive pressures; q= 5, and 10 MPa are shown in Figure 3. The applied axial compressive pressure is increased from left to right. It is worth noting that the effective stiffness, k_{eff}, reduces when the shear modulus, G_b, is decreased for every vertical condition (Table 4). In particular, the higher the applied axial compressive pressure, q is, the smaller the effective stiffness, k_{eff} is observed. It is worth noting that for $EB_{1,a}$, the effective stiffness is reduced by 10% when the applied axial compressive pressure is increased from 5 MPa to 10 MPa. Respectively, this decrease is 12.5%, 15%, and 25% for $EB_{1,b}$, $EB_{1,c}$, and $EB_{1,d}$. In addition, the damping ξ_{eff}, increases when the shear modulus, G_b, decreases: 18%, 12.5% and 10% for G_b from 0.66 MPa to 0.60 MPa. More discussion are shown in [42]. Overall, it is important to consider that these findings may have important applications when the inter-

action between the vertical loads and the horizontal forces become detrimental. For example, this may occur for bridges, tall buildings or structural configurations under severe lateral loads.

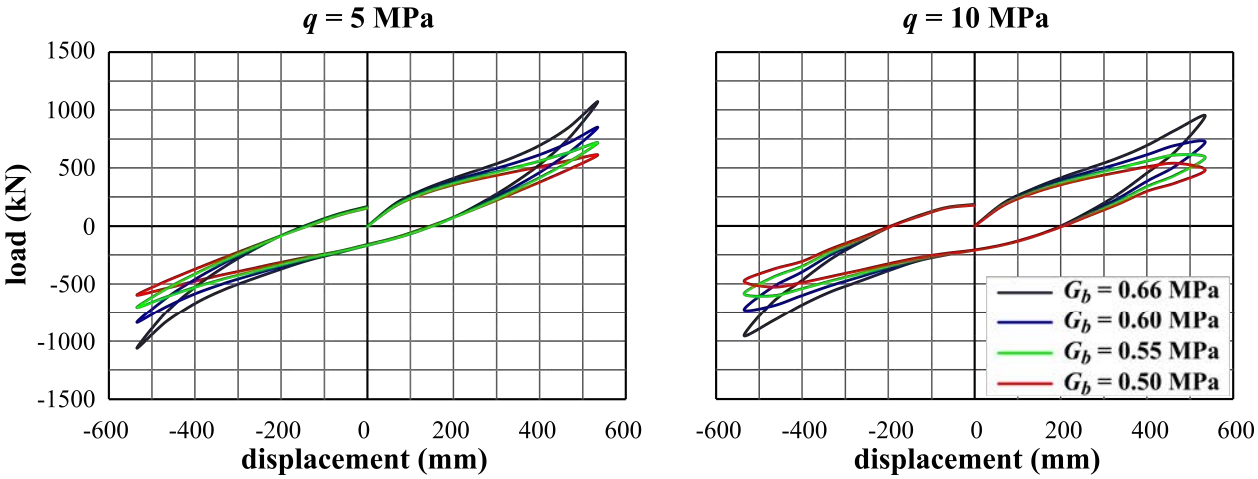

Figure 3. Load-displacement curves (hysteretic loops) of multiple EB numerical models; EB1, a, EB1, b, EB1, c, and EB1, d (Gb = 0.66, 0.60, 0.55 and 0.50 MPa, respectively), with: q= 5, and 10 MPa. The applied axial compressive pressure is increased from left to right.

shear modulus		axial compressive pressure	
G_b (MPa)		q= 5 MPa	q= 10 MPa
0.66	k_{eff} (kN/ mm)	2.0	1.8
($EB_{1, a}$)	ξ_{eff} (%)	6.8	10.2
0.60	k_{eff} (kN/ mm)	1.6	1.4
($EB_{1, b}$)	ξ_{eff} (%)	8.0	13.0
0.55	k_{eff} (kN/ mm)	1.3	1.1
($EB_{1, c}$)	ξ_{eff} (%)	9.0	15.3
0.50	k_{eff} (kN/ mm)	1.2	0.9
($EB_{1, d}$)	ξ_{eff} (%)	9.9	17.9

Table 4: Effective stiffness, keff, and damping ratio, ξeff, of the EB1, a, EB1, b, EB1, c, and EB1, d numerical models under applied axial compressive pressures of q= 5 and 10 MPa.

4 CONCLUSIONS

The paper performed 3D numerical simulations of elastomeric bearings (EB) subjected to the mutual interaction between horizontal and vertical loads. In particular, several load-displacement curves were produced for the various EB numerical models ($EB_{1,a}$, $EB_{1,b}$, $EB_{1,c}$, and $EB_{1,d}$), different G_b (0.66, 0.60, 0.55 and 0.50 MPa, respectively) and subjected to different applied axial compressive pressures; q= 5, and 10 MPa. The outcomes show that the shear modulus, Gb plays an important role in the in the increase of the effective stiffness, keff. On the other side, its effects on the damping ratio, ξeff, consist of a general reduction. Confirming previous literature contributions, the increase of the vertical pressure induces a decrease of the effective stiffness, keff, and increase of the damping ration, ξeff. However, these findings need to be limited to the configurations and assumptions that have been herein considered. The paper may have an important contribution in the improving of the seismic resilience of structural configurations.

REFERENCES

[1] Haringx, JA. 1948. "On highly compressible helical springs and rubber rods and their application for vibration-free mountings." *Philips Research Report*. **4**: 49-80.

[2] Kelly, J.M. 1997. *Earthquake-Resistant Design with Rubber*. Switzerland, Springer.

[3] Kelly, J.M., and D. Konstantinidis. 2009. "Steel shim stresses in multilayer bearings under compression and bending." *J. of Mech. of Materials and Str.* **4 (6)**: 1109–1125. DOI: https://doi.org/10.2140/jomms.2009.4.1109.

[4] Kelly, J.M., and D. Konstantinidis. 2011. *Mechanics of rubber bearings for seismic and vibration isolation*. New York: Wiley.

[5] Buckle, I., S. Nagarajaiah, and K. Ferrell. 2002. "Stability of elastomeric isolation bearings: Experimental study." *J. Struct. Eng.* **128(1)**: 3–11.

[6] Warn, G.P., A.S. Whittaker, and M. Constantinou. 2007. "Vertical stiffness of elastomeric and lead–rubber seismic isolation bearings." *J. Struct. Eng.* **133(9)**: 1227-1236.

[7] Benzoni, G.M., and C. Casarotti. 2008. *Performance of lead-rubber and sliding bearings under different axial load and velocity conditions*. No. SRMD-2006/05-rev3. California, California. Dept. of Transportation.

[8] Han, X., C.A. Kelleher, G.P. Warn, and T. Wagener. 2013. "Identification of the controlling mechanism for predicting critical loads in elastomeric bearings." *J. Struct. Eng.* **139(12)**: 04013016.

[9] Basagiannis, C. 2018. *Seismic design and evaluation of moment resisting frames using elastomeric dampers.* PhD Diss. Oxford, UK: University of Oxford.

[10] Ahmad, N., H. Shakeel, and M. Masoudi. 2020. "Design and development of low-cost HDRBs seismic isolation of structures." *Bull. of Earth. Eng.* **18(3)**: 1107-1138.

[11] Cardone, D., and G. Gesualdi. 2012. "Experimental evaluation of the mechanical behavior of elastomeric materials for seismic applications at different air temperatures." *Int. J. of Mech. Sciences.* **64(1)**: 127-143.

[12] Rastgoo Moghadam, S., and D. Konstantinidis. 2021. "Experimental and analytical studies on the horizontal behavior of elastomeric bearings under support rotation." *J. Struct. Eng.* **147(4)**: 04021024.

[13] Nagarajaiah, S., and K. Ferrell. 1999. "Stability of elastomeric seismic isolation bearings." *J. Struct. Eng.* **125(9)**: 946-954.

[14] Kumar, M., A.S. Whittaker, and M. Constantinou. 2014. "An advanced numerical model of elastomeric seismic isolation bearings." *Earth. Eng. and Str. Dyn*. **43(13)**: 1955-1974.

[15] Rastgoo Moghadam, S., and D. Konstantinidis. 2017. "Finite element study of the effect of support rotation on the horizontal behavior of elastomeric bearings." *Compos. Struct.* **163**: 474–490. DOI: https://doi.org /10.1016/j.compstruct.2016.12.013.

[16] Kalfas, K.N., S.A. Mitoulis, and K. Katakalos. 2017. "Numerical study on the response of steel-laminated elastomeric bearings subjected to variable axial loads and development of local tensile stresses." *Eng. Struct*. **134**: 346-357. DOI: https://doi.org/10.1016/j.engstruct.2016.12.015

[17] Kalfas, K.N., S.A. Mitoulis, and K. Katakalos. 2017. "Numerical study on bridge elastomeric bearings subjected to large shear strains with emphasis on local tension." In *Proc., 16th World Conf. on Earthquake Engineering*. Tokyo: International Association for Earthquake Engineering.

[18] Kalfas, K.N., S.A. Mitoulis, and D. Konstantinidis. 2020. "Influence of steel reinforcement on the performance of elastomeric bearings." *J. Struct. Eng.* **146(10)**: 04020195. DOI: 10.1061/(ASCE)ST.1943-541X.0002710.

[19] Kalfas, K.N., and S.A. Mitoulis. 2017. "Performance of steel-laminated rubber bearings subjected to combinations of axial loads and shear strains." *Procedia Eng*. **199**: 2979-2984. DOI: https://doi.org/10 .1016/j.proeng.2017.09.533.

[20] Forcellini, D. 2018. "Seismic assessment of a benchmark based isolated ordinary building with soil structure interaction." *Bull. of Earth. Eng*. **16(5)**: 2021-2042.

[21] Forcellini. 2022 "The assessment of the interaction between base isolation (BI) technique and soil structure interaction (SSI) effects with 3D numerical simulations", *Structures* **45** (2022) 1452–1460

[22] Forcellini, D., and K.N. Kalfas. 2023. "Inter-story seismic isolation for high-rise buildings." *Engineering Structures* **275**: 115175.

[23] Gauron, O., A. Saidou, A. Busson, and G.H. Siqueira. 2018. "Experimental determination of the lateral stability and shear failure limit states of bridge rubber bearings." *Eng. Struct*. **174**: 39-48. DOI: https://doi.org/10.1016/j.engstruct.2018.07.039.

[24] Forcellini, D. 2018. "Cost Assessment of isolation technique applied to a benchmark bridge with soil structure interaction." *Bull. of Earth. Eng*. **15(1)**: 51-69.

[25] Forcellini, D. 2016. "3D Numerical simulations of elastomeric bearings for bridges." *Innovative Infrastructure Solution*. **1(1)**: 45.

[26] Kalfas, K.N., and D. Forcellini. 2020. "A developed analytical non-linear model of elastomeric bearings verified with numerical findings." In *Proc*., *Eurodyn*, *XI Int. Conf. on Structural Dynamics*. Athens, Greece: The European Association for Structural Dynamics.

[27] Rahnavard, R., and R.J. Thomas. 2019. "Numerical evaluation of steel-rubber isolator with single and multiple rubber cores." *Eng. Struct.* **198**: 109532.

[28] Altalabani, D., F. Hejazi, R.S. Bin Muhammad Rashid, F.N.A. Abd Aziz. 2021. "Development of new rectangular rubber isolators for a tunnel-form structure subjected to seismic excitations." *Structures*. **32**: 1522–1542.

[29] Sheikhi, J., M. Fathi, and R. Rahnavard. 2020 "Natural rubber bearing incorporated with high toughness steel ring dampers." *Structures*. **24**: 107-123. https://doi.org/10.1016/j.istruc.2020.01.013.

[30] Sheikhi, J., M. Fathi, R. Rahnavard, and R. Napolitano. 2021. "Numerical analysis of natural rubber bearing equipped with steel and shape memory alloys dampers." *Structures*. **32**:1839-1855. https://doi.org/10.1016/j.istruc.2021.03.115.

[31] Radkia, S., R. Rahnavard, H. Tuwair, F.A. Gandomkar, and R. Napolitano. 2020 "Investigating the effects of seismic isolators on steel asymmetric structures considering soil-structure interaction.", *Structures*. **27**: 1029-1040. https://doi.org/10.1016/j.istruc.2020.07.019.

[32] Crowder, A.P., and T.C. Becker. 2017. "Experimental investigation of elastomeric isolation bearings with flexible supporting columns." *J. Struct. Eng.* **143 (7)**: 04017057. DOI: https://doi.org/10.1061/(ASCE)ST.1943-541X.0001784.

[33] Forcellini, D., S.A. Mitoulis, and K.N. Kalfas. 2017. "Study of the response of elastomeric bearings with 3D numerical simulations and experimental validation." *In Proc., 6th Int. Conf. on Computational Methods in Structural Dynamics and Earthquake Engineering*. 569–577. Rhodes Island, Greece.

[34] Van Engelen, N.C. 2019. "Rotation in rectangular and circular reinforced elastomeric bearings resulting in lift-off." *Int. J. of Solids and Str.* **168**: 172-182.

[35] Bai, J., N. C. Van Engelen, and S. Cheng. 2021. "Parametric studies on the behaviour of reinforced elastomeric bearings considering the compressibility and extensibility index, shape factor, and lift-off." *Structures*. **31**: 1278-1286.

[36] Takahashi, Y. 2012. "Damage of rubber bearings and dampers of bridges in 2011 Great East Japan earthquake." In *Proc., Int. Symp. on Engineering Lessons Learned from the 2011 Great East Japan Earthquake*, 1333–1342. Tokyo: International Association for Earthquake Engineering.

[37] Kwon, O.S., and S.H. Jeong. 2013. "Seismic displacement demands on skewed bridge decks supported on elastomeric bearings." *J. Earth. Eng.* **17 (7)**: 998–1022. https://doi.org/10.1080/13632469.2013.791894

[38] EN 1998-2. 2005. *Eurocode 8: Design of structures for earthquake resistance. Part 2: Bridges*. EN 1998-2. Brussels, Belgium: European Committee for Standardization.

[39] AASHTO. 2014. *Guide specifications for seismic isolation design*. 4th ed. Washington, DC: AASHTO.

[40] Forcellini, D., and J.M. Kelly. 2014. "Analysis of the large deformation stability of elastomeric bearings." *J. Eng. Mech.* **140(6)**: 04014036.

[41] Koh, C.G., and J.M. Kelly. 1988. "A simple mechanical model for elastomeric bearings used in base isolation." *Int. J. of Mech. Sciences.* **30(12)**: 933-943.

[42] Kalfas KN, Ghorbani Amirabad N, Forcellini D. 2021. "The role of shear modulus on the mechanical behavior of elastomeric bearings when subjected to combined axial and shear loads." *Eng Struct* **248**: 113248. https://doi.org/10.1016/j. engstruct.2021.113248.

[43] Kalfas KN, Forcellini D. 2021. *Analytical formulas of the mechanical behavior of rubber bearings considering the isolator nonlinearities and the influence of shear modulus*. In *Seismic Evaluation, Damage, and Mitigation in Structures*, pp. 343-363. Woodhead Publishing.

[44] Dassault Systèmes. 2014. *ABAQUS/CAE 6.13 user's manual. Abaqus Ver. 6.13 documentation*. Providence, RI: Dassault Systèmes.

[45] Ogden, W.R. 1972. "Large deformation isotropic elasticity – On the correlation of theory and experiment for incompressible rubberlike solids." *Proc. of the Royal Soc. of London. Series A, Math. and Ph. Sciences.* **326:** 565–584.

[46] Boulanger, P., and M. Hayes. 2001. *Finite-amplitude waves in Mooney-Rivlin and Hadamard materials*. *Topics in finite elasticity*. Vienna: Springer: 131-167.

[47] Rivlin, R.S. 1948. "Large elastic deformations of isotropic materials IV. Further developments of the general theory." *Philosophical Transactions of the Royal Society of London. Series A, Mathematical and Physical Sciences*. **241(835)**: 379-397.

[48] Kim, B., S.B. Lee, J. Lee, S. Cho, H. Park, S. Yeom, and S.H. Park. 2012. "A comparison among Neo-Hookean model, Mooney-Rivlin model, and Ogden model for chloroprene rubber." *International Journal of Precision Engineering and Manufacturing*. **13(5)**: 759-764.

[49] Bergström, J.S., and M.C. Boyce. 1998. "Constitutive Modeling of the Large Strain Time-Dependent Behavior of Elastomers." *J. of Mechanics and Physics of Solids.* **46**: 931-954.